Astronomy
&
Astrophysics

Abundant gas-phase H₂O in absorption toward massive protostars[*]

A. M. S. Boonman[1] and E. F. van Dishoeck[1]

Sterrewacht Leiden, PO Box 9513, 2300 RA Leiden, The Netherlands

Abstract. We present infrared spectra of gas-phase H_2O around 6 μm toward 12 deeply embedded massive protostars obtained with the Short Wavelength Spectrometer on board the Infrared Space Observatory (ISO). The ν_2 ro-vibrational band has been detected toward 7 of the sources and the excitation temperatures indicate an origin in the warm gas at $T_{ex} \gtrsim 250$ K. Typical derived gas-phase H_2O abundances are $\sim 5 \times 10^{-6} - 6 \times 10^{-5}$, with the abundances increasing with the temperature of the warm gas. The inferred gas/solid ratios show a similar trend with temperature and suggest that grain-mantle evaporation is important. The increasing gas/solid ratio correlates with other indicators of increased temperatures. If the higher temperatures are due to a larger ratio of source luminosity to envelope mass, this makes gas-phase H_2O a good evolutionary tracer. Comparison with chemical models shows that three different chemical processes, ice evaporation, high-T chemistry, and shocks, can reproduce the high inferred gas-phase H_2O abundances. In a forthcoming paper each of these processes are investigated in more detail in comparison with data from the Long Wavelength Spectrometer on board ISO and the Submillimeter Wave Astronomy Satellite (SWAS). Comparison with existing SWAS data indicates that a jump in the H_2O abundance is present and that the observed ν_2 ro-vibrational band traces primarily the warm inner envelope.

Key words. ISM: abundances – ISM: molecules – molecular processes – stars: formation – stars: circumstellar matter – infrared: ISM

1. Introduction

In recent years, many gas-phase H_2O lines have been detected toward star-forming regions. Prior to the Infrared Space Observatory (ISO), only a few H_2O and/or isotopic lines had been observed at submillimeter wavelengths (e.g. Phillips et al. 1980; Cernicharo et al. 1994; Zmuidzinas et al. 1995; Gensheimer et al. 1996). Observations of intermediate- to high-mass protostars with the Short Wavelength Spectrometer (SWS) on board ISO have led to the detection of more than 30 different ro-vibrational H_2O absorption lines around 6 μm (van Dishoeck & Helmich 1996; Dartois et al. 1998; González-Alfonso et al. 1998). The advantage of infrared absorption measurements is that many lines can be observed at the same time in a pencil beam toward the infrared source. This allows a much more accurate determination of the gas-phase H_2O abundance than from submillimeter emission lines observed within different beams. The disadvantage is the low spectral resolution of ISO of $\lambda/\Delta\lambda \sim 1400$ around 6 μm, so that

absorption can only be detected toward sources with intrinsic line widths of at least a few km s^{-1}. In addition, no kinematical information can be derived from the data.

Abundances of up to $\sim 10^{-4}$ have been detected with ISO toward intermediate- to high-mass star-forming regions (van Dishoeck & Helmich 1996; van Dishoeck 1998; Nisini et al. 1999; Ceccarelli et al. 1999). These are in agreement with a variety of chemical models, including high-T chemistry and shocks, which predict enhanced H_2O abundances for $T \gtrsim 230$–300 K where most of the oxygen is driven into H_2O, as well as grain-mantle evaporation predicting enhanced H_2O abundances for $T \gtrsim 100$ K (Charnley 1997; Doty et al. 2002). On the other hand, observations of the H_2O $1_{10}-1_{01}$ line at 557 GHz obtained in a large ($\sim 4'$) beam with the Submillimeter Wave Astronomy Satellite (SWAS) show much lower gas-phase abundances of $\sim 10^{-9}$ to a few 10^{-8} in the cold ($T \lesssim 50$ K) gas (Snell et al. 2000; Ashby et al. 2000).

So far, most studies of gas-phase H_2O have focussed on a single or a few source(s). In this paper, we present the analysis of the ν_2 ro-vibrational band of gas-phase H_2O around ~ 6 μm toward 12 deeply embedded massive protostars. The larger sample presented here allows investigation of general evolutionary trends. A detailed analysis of this ro-vibrational H_2O band in combination with pure rotational lines observed

Table 1. Observed sources.

Source	RA (2000)	DEC (2000)	Observation ID	6 μm Flux[a] (Jy)	Luminosity $10^5 L_\odot$	Distance (kpc)	Reference[b]
AFGL 2591	20^h 29^m 24^s.4	+40° 11′ 19″	35701221	520	0.2	1	1, 1
AFGL 2136	18^h 22^m 26^s.4	−13° 30′ 08″	31101023	150	0.7	2	1, 1
AFGL 4176	13^h 43^m 02^s.4	−62° 08′ 52″	11701605	175	1.8	4	2, 3
MonR2 IRS3	06^h 07^m 48^s.4	−06° 22′ 55″	71101802	150	0.13	0.95	4, 5
NGC 7538 IRS 1	23^h 13^m 45^s.4	+61° 28′ 09″	28301235	100	1.3	2.8	1, 1
NGC 7538 IRS 9	23^h 14^m 01^s.4	+61° 27′ 20″	09801533	35	0.4	2.8	1, 1
NGC 2024 IRS 2	05^h 41^m 45^s.4	−01° 54′ 34″	66701228	45	1	0.4	6, 7
AFGL 2059	18^h 04^m 53^s.4	−24° 26′ 45″	49302585	70	0.16	1.5	2, 3
NGC 3576	11^h 11^m 53^s.4	−61° 18′ 25″	29200143	60	3.5	2.4	2, 8
S 140 IRS 1	22^h 19^m 18^s.4	+63° 18′ 47″	26301731	180	0.2	0.9	1, 1
W 33 A	18^h 14^m 39^s.4	−17° 52′ 01″	46700521	25	1.0	4	1, 1
W 3 IRS 5	02^h 25^m 40^s.4	+62° 05′ 52″	80002247	200	1.7	2.2	1, 1

[a] Continuum flux at ~6.5 μm.

[b] The first reference refers to the luminosity, the second to the distance.

References: 1. Van der Tak et al. (2000b); 2. Lahuis & van Dishoeck (2000); 3. Henning et al. (1990); 4. Henning et al. (1992); 5. Giannakopoulou et al. (1997); 6. Thompson et al. (1981); 7. Anthony-Twarog (1982); 8. Persi et al. (1987).

with SWAS and the Long Wavelength Spectrometer (LWS) on board ISO toward a sub-set of this sample will be presented in a forthcoming paper (Boonman et al. 2003b; hereafter Paper II).

All sources in our sample have luminosities between ~10^4–10^5 $L_\odot$ and have been studied before in other gas-phase molecules, both at infrared and submillimeter wavelengths (e.g. Lahuis & van Dishoeck 2000; Boonman et al. 2003a; van der Tak et al. 2003). In addition, solid-state features of H$_2$O, CO$_2$ and ^{13}CO$_2$ toward the same sources have been analyzed (Keane et al. 2001b; Gerakines et al. 1999; Boogert et al. 2000). The reduction of the data is described in Sect. 2. Section 3 describes the analysis of the spectra, using pure absorption models, and radiative transfer effects are investigated in Sect. 4. Finally, the results are discussed in Sect. 5 and the conclusions presented in Sect. 6.

2. Observations and reduction

The observations of the ν_2 ro-vibrational band of gas-phase H$_2$O around 6 μm have been performed with ISO-SWS in the AOT6 grating mode, and are summarized in Table 1. The spectra toward all sources have been reduced with the ISO-SWS Interactive Analysis System SIA using the ISO Off-line Processing (OLP version 7) software modules and calibration files. Later versions of this Off-line Processing software (OLP versions 8 to 10) have been checked and no significant improvements are found. Unlike at other wavelengths, the 5–7 μm region is relatively free from instrumental fringes, but since defringing does improve the signal-to-noise ratio, a cosine has been fitted to the data (Lahuis & van Dishoeck 2000). The depths of the H$_2$O lines with and without fringe removal have been compared to make sure that the H$_2$O lines are not partially removed by the defringing routine.

The spectra have been rebinned to an effective spectral resolution of $\Delta\lambda = 0.0042$ μm. These spectra have been divided by a manual fit to the H$_2$O ice band resulting in the normalised spectra presented in Fig. 1. The 1σ noise level in the final spectra is typically 1–3% of the continuum, with the lowest noise level corresponding to the sources with the highest continuum flux (Table 1). The higher noise level between ~5.7 and 6.2 μm toward W 33 A is due to the presence of a strong H$_2$O ice band resulting in a sharp drop in the continuum to ~10 Jy.

The ν_2 ro-vibrational band of gas-phase H$_2$O has been detected toward the sources AFGL 2591, AFGL 2136, AFGL 4176, MonR2 IRS3, AFGL 2059 (M8E-IR), NGC 3576, and W 3 IRS5. For AFGL 2591, AFGL 4176, and W 3 IRS5 the SWS AOT6 observations in parallel with the AOT7 Fabry-Pérot scans have been used, since these have a slightly better signal-to-noise ratio. For sources for which multiple observations exist, the features are very reproducable. The spectra toward some of our sources have been analysed previously by van Dishoeck & Helmich (1996), Helmich et al. (1996), and van Dishoeck (1998). The reduced spectra presented here are however of a higher quality, since both the instrument calibration and the reduction routines have significantly improved for the 5–7 μm wavelength region compared to those used in 1996. Also, the wavelength range shown here is somewhat larger than in van Dishoeck & Helmich (1996), resulting in the detection of more H$_2$O absorption lines, especially between 6.6 and 7 μm. The detection of the ν_2 ro-vibrational band of gas-phase H$_2$O toward 7 sources and useful upper limits for the other massive protostars will allow to search for evolutionary trends.

3. Analysis

3.1. Comparison of the spectra

The spectra in Fig. 1 are ordered according to a decreasing temperature of the warm gas, with the warmest sources at the top, using $T_{\rm ex}(C_2H_2)$ as a temperature indicator (Lahuis & van Dishoeck 2000). Generally, the strongest H$_2$O absorption is found for the warmest sources. For example, the broad
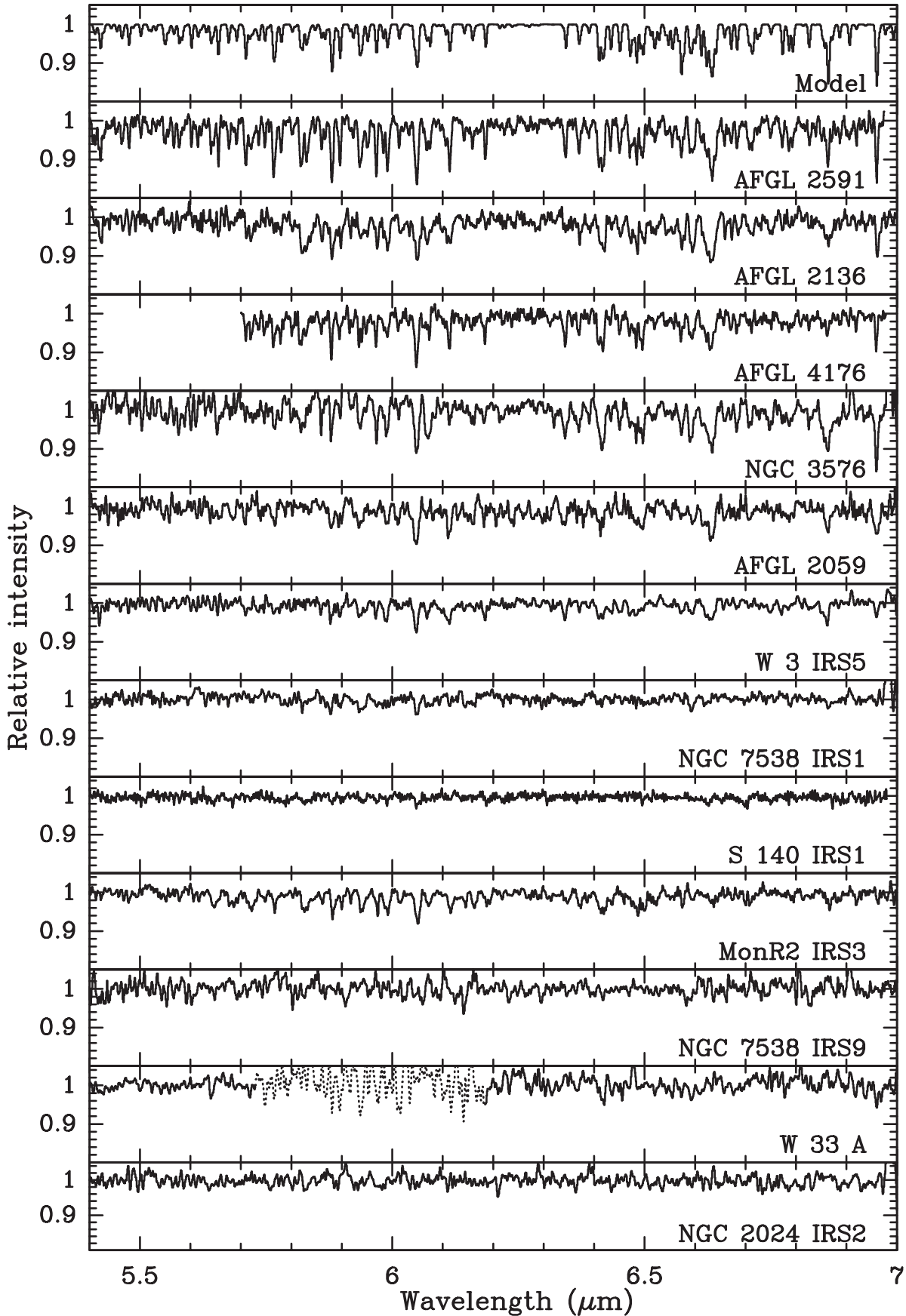
Fig. 1. Normalised ISO-SWS spectra of the ν_2 ro-vibrational band of gas-phase H_2O for all sources. The H_2O ice feature has been removed. The ~5.7–6.2 μm region toward W 33 A is particularly noisy due to the strong H_2O ice band for this source. The bottom panel shows a H_2O model spectrum for $T_{ex} = 500$ K, $N = 2 \times 10^{18}$ cm^{-2}, and $b = 5$ km s^{-1} (see Sect. 3).

feature around 6.63 μm appears to be strongest for these sources. This feature is a blend of several gas-phase lines with energy levels $\gtrsim$200 K, which can explain its absence in the cooler sources. The warmer sources generally show more lines for $\lambda \gtrsim$ 6.5 μm, which correspond to P-branch lines from higher-J levels. However, no gradual decrease of the absorption depth of the ν_2 ro-vibrational band with decreasing temperature is seen.

Most of the narrow absorption lines are in fact blends of two or more lines arising from different energy levels, making it difficult to find trends. The lines at ~6.05 and ~6.12 μm, which include the transitions from the ground-states of ortho- and para-H$_2$O respectively, are clearly present in all sources where the ν_2 ro-vibrational band is detected. In NGC 7538 IRS1 and S 140 IRS1, where no detection is claimed, there is a hint of the ground-state line of ortho-H$_2$O.

The sources in which the ν_2 ro-vibrational band of gas-phase H$_2$O is detected show all lines in absorption. Analysis of the same band toward Orion-IRc2 shows the R-branch lines, with $\lambda \lesssim$ 6.2 μm, in absorption, whereas the P-branch ($\lambda \gtrsim$ 6.2 μm) is in emission (González-Alfonso et al. 1998). For this reason, we have not included Orion-IRc2 in the analysis of the sample.

3.2. Pure absorption models

The spectra have been modeled using the method described in Lahuis & van Dishoeck (2000). In this method, synthetic spectra are computed assuming that only absorption takes place and that emission can be neglected. The effects of emission filling in the absorption are discussed in Sect. 4. The source is assumed to be a homogeneous sphere with a single temperature T_{ex} and column density N, and the molecular line data from the HITRAN 2000 database (http://www.hitran.com) are used. The models are more sensitive to the H$_2$O line width than those for other molecules. Therefore, line widths of $b \sim$ 1.5–10 km s^{-1} have been investigated. The resulting synthetic spectra have been convolved to the nominal spectral resolution of the ISO-SWS spectra for comparison with the data.

The best fit to the data has been determined using the reduced χ_ν^2-method. Figure 2 shows an example of χ_ν^2 contours for the source MonR2 IRS3 for different line widths. This figure illustrates that for low b-values (i.e. $b \lesssim$ 2 km s^{-1}) the temperature and column density of gas-phase H$_2$O are not well constrained. In the following analysis a line width of $b = 5$ km s^{-1} is adopted for H$_2$O. This corresponds to the mean value of the ^{13}CO $v = 1$–0 absorption line widths found by Mitchell et al. (1990). For $b = 5$ km s^{-1}, the column density of gas-phase H$_2$O is well constrained, but the excitation temperature shows a larger spread than for the CO$_2$, HCN, and C$_2$H$_2$ absorption bands using a similar analysis (Boonman et al. 2003a; Lahuis & van Dishoeck 2000). This is due to the absence of a Q-branch in the ν_2 ro-vibrational band of H$_2$O. The best fitting model parameters for all sources are listed in Table 2 and Fig. 3 shows some good fitting H$_2$O model spectra for the source MonR2 IRS3.
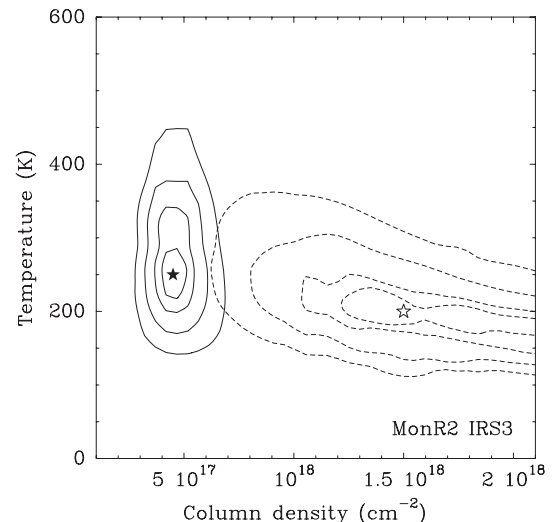

Fig. 2. Example of the χ^2 distribution for MonR2 IRS3 for $b = 5$ km s^{-1} (filled star and solid contours) and $b = 2$ km s^{-1} (open star and dashed contours) showing that for low b-values ($b \lesssim 2$ km s^{-1}) the column density is not well constrained. The stars indicate the minimum χ^2 and the contours are 0.2, 1, 3, and 6% above this minimum. The latter contour roughly corresponds to a 3σ deviation of the model from the observed H$_2$O band for this source.

Table 2. Model parameters for the ν_2 band of gas-phase H$_2$O[a].

Source	T_{ex}(H$_2$O) K	N(H$_2$O) 10^{18} cm^{-2}	N(H$_2^{hot}$)[b] 10^{22} cm^{-2}	x(H$_2$O)[c] 10^{-5}
AFGL 2591	450^{+250}_{-150}	3.5 ± 1.5	6.0	5.8
AFGL 2136	500^{+250}_{-150}	1.5 ± 0.6	7.5	2.0
AFGL 4176	400^{+250}_{-250}	1.5 ± 0.7	4.0	3.8
MonR2 IRS3	250^{+200}_{-100}	0.5 ± 0.2	2.2[d]	2.3
NGC 7538 IRS1	500[e]	< 0.5	4.1	< 1.2
NGC 7538 IRS9	300[f]	< 0.6	0.1	< 60
NGC 2024 IRS2	45[g]	< 0.3	–	–
AFGL 2059	500^{+300}_{-300}	0.6 ± 0.3	2	3
NGC 3576	500^{+250}_{-250}	0.9 ± 0.3	4	2.3
S 140 IRS1	390[h]	< 0.3	2.2	< 1.4
W 33 A	120[h]	< 0.8	6.9	< 1.2
W 3 IRS5	400^{+200}_{-150}	0.3 ± 0.1	6.2	0.5

[a] For $b = 5$ km s^{-1}.
[b] From Lahuis & van Dishoeck (2000), unless otherwise noted.
[c] N(H$_2$O)/N(H$_2^{hot}$).
[d] Using N(^{13}CO) from Giannakopoulou et al. (1997), adopting ^{12}CO/^{13}CO = 60 and ^{12}CO/H$_2$ = 2×10^{-4}.
[e] T_{ex}(C$_2$H$_2$) from Boonman et al. (2003a).
[f] T_{ex}(C$_2$H$_2$) from Lahuis & van Dishoeck (2000).
[g] T_{ex}(^{12}CO) from Lacy et al. (1994).
[h] T_{ex}(^{13}CO) from Mitchell et al. (1990).

The results show that the detected H$_2$O gas is warm ($T_{ex} >$ 250 K), but that there is not a clear correlation with T_{ex}(C$_2$H$_2$) (Fig. 4). This is probably caused by the large error bars on the H$_2$O excitation temperature. Van der Tak (2000) argues that the dust opacity at 6 μm is comparable to that at 13 μm, near the C$_2$H$_2$ absorption band. This would imply that the lack of
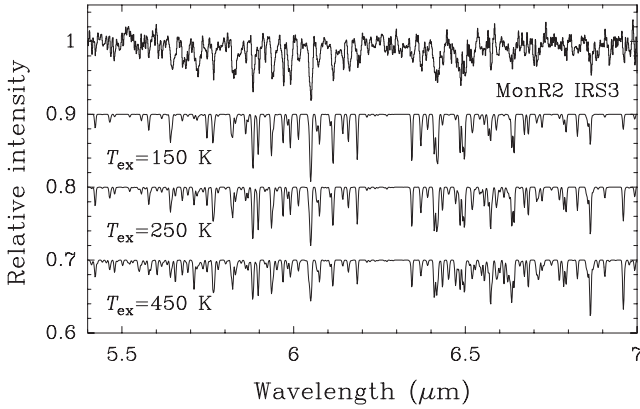
Fig. 3. Example of some good fitting models for the observed ν_2 ro-vibrational band of gas-phase H$_2$O toward MonR2 IRS3, for different excitation temperatures using $b = 5$ km s^{-1} and $N = 5 \times 10^{17}$ cm^{-2} (Table 2). The model spectra are shifted by -0.1, -0.2, and -0.3 respectively (from top to bottom).

a clear correlation between $T_{\rm ex}$(C$_2$H$_2$) and $T_{\rm ex}$(H$_2$O) is likely not caused by hot gas-phase H$_2$O hidden behind an opaque dust layer. Plotting $T_{\rm ex}$(H$_2$O) versus $T_{\rm ex}$(CO) of the warm gas from Mitchell et al. (1990) shows the same lack of a clear correlation. Figure 9 of Lahuis & van Dishoeck (2000) shows that overall there is a good correlation between the CO and C$_2$H$_2$ temperatures. In general, $T_{\rm ex}$(C$_2$H$_2$) is preferred as a tracer of the inner warm envelope because it suffers less from confusion by outflow material, and because the absorption of this molecule is enhanced in the inner region.

3.3. Abundances

The derived H$_2$O column densities have been converted into abundances with respect to the warm H$_2$ gas, since the spectra show primarily warm H$_2$O gas at $T_{\rm ex} > 250$ K. The H$_2$ column densities in the warm gas have been derived from infrared observations of ^{13}CO (e.g. Mitchell et al. 1990). A ^{12}CO/^{13}CO ratio of 60 and a ^{12}CO/H$_2$ ratio of 2×10^{-4} have been assumed (Lahuis & van Dishoeck 2000; Lacy et al. 1994). Typical derived gas-phase H$_2$O abundances are $\sim 5 \times 10^{-6}$–6×10^{-5}, increasing with temperature (Fig. 5; Table 2). The derived H$_2$O abundances for AFGL 2591, AFGL 2136, AFGL 4176, and NGC 7538 IRS9 agree well with those previously derived by van Dishoeck & Helmich (1996), but the derived H$_2$O excitation temperatures for these sources seem somewhat higher than their adopted value of $T_{\rm ex} = 300$ K (Table 2).

The H$_2$O ice abundances with respect to cold H$_2$ gas are shown in Fig. 5 for comparison and are seen to decrease with temperature. Using $T_{\rm ex}$(H$_2$O) instead of $T_{\rm ex}$(C$_2$H$_2$) in Fig. 5 shows the same trends, although somewhat steeper. This suggests that grain mantle evaporation plays an important role in the production of gas-phase H$_2$O.

The gas-phase abundance in the warmest source is still a factor of ~ 3.5 lower than the ice abundance in the coldest source. If the gas-phase H$_2$O results from evaporation of ice mantles, they are expected to be the same. The difference may have several reasons. First, the adopted b-value may be too large. Adopting a lower b-value for which the column density is
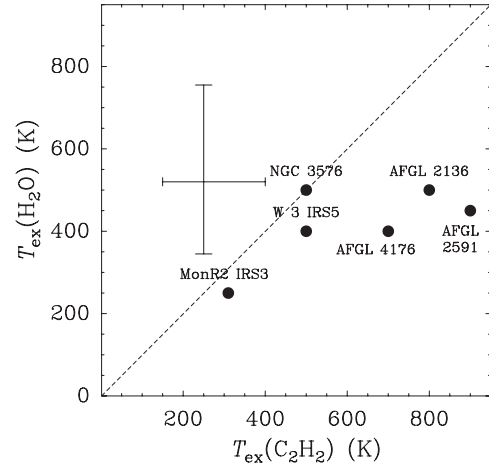

Fig. 4. Correlation between the H$_2$O excitation temperature and that of C$_2$H$_2$, a good tracer of the warm gas (Lahuis & van Dishoeck 2000). Only those sources are shown for which both excitation temperatures are determined, except for MonR2 IRS3 for which $T_{\rm ex}$(^{13}CO) instead of $T_{\rm ex}$(C$_2$H$_2$) is used (Giannakopoulou et al. 1997). The cross denotes typical error bars.

still well-constrained ($b > 2$ km s^{-1}), may increase the inferred abundances by factors of ≤ 1.5. Second, part of the H$_2$O absorption may originate in cold H$_2$O gas. Using the total H$_2$ column density instead of the warm component only, results in a factor of ~ 2.3 lower H$_2$O abundances in the gas-phase compared to the ices. Fitting a two-temperature component model to the data, using the ^{13}CO temperatures for the warm and cold gas, shows that column densities up to $\sim 10^{18}$ cm^{-2} could be present in cold H$_2$O gas at $T \leq 100$ K. Such large amounts of cold gas should have been picked up with the SWAS satellite, which is not the case (see Paper II). Therefore, it is not likely that the cold H$_2$O gas below ~ 100 K contributes significantly to the observed absorption spectra. A third possibility is that H$_2$O may be destroyed in the gas-phase after evaporation from the grains. Current models of gas-phase chemistry predict production of gas-phase H$_2$O in warm regions rather than destruction (e.g. Charnley 1997). On the other hand, processes like X-ray dissociation may be able to destroy some gas-phase H$_2$O in the warmest regions close to the central radiation source, but this is not likely to be a significant fraction (see Boonman et al. 2003a).

Finally, both the assumption of pure absorption and of a homogeneous source with a constant temperature and column density may underestimate the H$_2$O abundance in the warm gas. The effect of emission filling in the absorption is discussed in Sect 4. In Paper II it will be shown that combining the inferred temperature and density gradients from van der Tak et al. (2000b) with a detailed chemical model, results in H$_2$O abundances of $\sim 10^{-4}$ in the warm gas and can successfully explain the observed ro-vibrational spectrum of gas-phase H$_2$O. Therefore, the difference between the gas-phase H$_2$O abundance in the warmest source and the ice abundance in the coldest source is probably due to both the assumption of pure absorption and of a homogeneous source with a constant excitation temperature and column density in the current models.
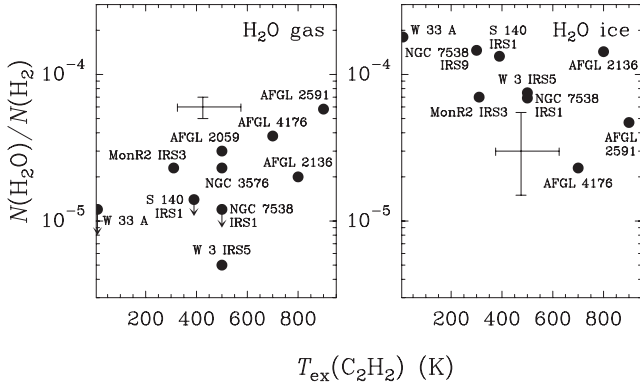
Fig. 5. The H_2O gas-phase abundances from Table 2 (left panel) and the H_2O ice abundances from Gibb & Whittet (2002) and Gerakines et al. (1999) (right panel) versus $T_{ex}(C_2H_2)$ (Lahuis & van Dishoeck 2000; Boonman et al. 2003a). The ice abundances are with respect to cold H_2 only, inferred from the cold ^{13}CO component from Mitchell et al. (1990) in a similar way as for the warm component (see text). The crosses denote typical error bars for $T_{ex} \gtrsim 200$ K. For MonR2 IRS3 and S 140 IRS1 $T_{ex}(^{13}CO)$ is used (Giannakopoulou et al. 1997; Mitchell et al. 1990).

Fig. 6. Gas/solid ratio for H_2O versus $T_{ex}(C_2H_2)$. For MonR2 IRS3 and S 140 IRS1 $T_{ex}(^{13}CO)$ is used (Giannakopoulou et al. 1997; Mitchell et al. 1990). The dashed line shows the least-squares fit through the data points.

3.4. Gas/solid ratios

The derived gas-phase H_2O abundances from Table 2 can be combined with the corresponding ice abundances from Gibb & Whittet (2002) and Gerakines et al. (1999) to determine the gas/solid ratios. Figure 6 shows that these ratios increase with temperature. A similar trend is seen for CO_2 (Boonman et al. 2003a). Using $T_{ex}(H_2O)$ instead of $T_{ex}(C_2H_2)$ in Fig. 6 shows a similar, but somewhat steeper trend.

The low gas/solid ratios generally correspond to those sources for which the ν_2 ro-vibrational band of gas-phase H_2O is not detected. This indicates that for those sources either most of the H_2O is still on the grains or that the line widths for these sources are smaller than the adopted $b = 5$ km s⁻¹. A smaller line width can increase the inferred gas/solid ratios for the colder sources by a factor of a few, but will not change the general increase of the gas/solid ratio with temperature. The observed trend in the gas/solid ratio emphasizes the result from Fig. 5 that grain mantle evaporation plays a role.

4. Radiative transfer effects

In the previous sections it is assumed that only absorption takes place, but especially in the warm gas, emission may fill in the absorption. For example, toward Orion-IRc2 part of the H_2O ν_2 band appears in emission (González-Alfonso et al. 1998). In order to investigate this effect, an excitation model has been set-up using rotational energy levels up to $E \sim 760$ cm⁻¹ in the ground state and $E \sim 1500$ cm⁻¹ in the first vibrationally excited state. The level populations are calculated adopting a Boltzmann distribution using T_{ex} from Table 2. As central radiation source, a blackbody is adopted for each object at a temperature ~ 100 K higher than the inferred H_2O exci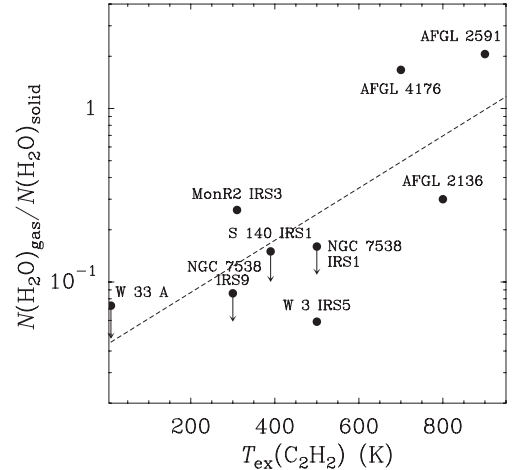tation temperature, to maximize the effect of emission filling in the absorption lines. If the blackbody temperature is taken equal to $T_{ex}(H_2O)$ the P-branch lines appear in emission, while the R-branch lines are still in absorption similar to what is observed toward Orion-IRc2 (González-Alfonso et al. 1998). However, our sources do not show such a phenomenon. This is probably due to their larger distances compared to Orion allowing a much smaller part of the beam being filled with emission. This emission will be more beam-diluted and thus more difficult to detect.

Adopting a homogeneous source with a constant temperature and density as in Sect. 3 for $b = 5$ km s⁻¹, shows that emission starts filling in the absorption significantly for $T_{ex} \gtrsim 250$ K. The resulting column densities are a factor of ~ 3–6 higher than in the case of pure absorption.

Van der Tak et al. (2000b) and Mueller et al. (2002) have shown that temperature and density gradients are present in the envelopes of the massive protostars studied here. Adopting the physical structure from van der Tak et al. (2000b) and assuming a Boltzmann distribution in each shell with T_{ex} equal to the dust temperature in that shell increases the inferred column density by similar factors as in the case of a constant temperature and density.

These factors can easily account for the difference between the H_2O gas-phase abundances for the warmest sources and the H_2O ice abundances in the coldest sources. Since the inclusion of emission enhances the abundances in particular for the warmest sources, this effect also preserves the inferred trends with temperature for the gas-phase H_2O abundances and gas/solid ratios (see Sect. 3). It should be noted that it is difficult to derive accurate abundances when emission is included, since they depend on the adopted central radiation source. If, e.g., the blackbody temperature is taken equal to the dust sublimation temperature of $T \sim 1400$ K, the inferred column densities increase by only a factor of $\lesssim 2$.

5. Discussion

5.1. H_2O as an evolutionary tracer

In Sect. 3 it is found that both the inferred gas-phase H_2O abundances and the gas/solid ratios increase with the temperature of the warm gas, while the H_2O ice abundances decrease. This indicates that H_2O is a good tracer of the warm gas. Higher temperatures throughout the envelope are likely due to a higher ratio of the source luminosity to the envelope mass, which may correspond to dispersion of a larger fraction of the envelope (van der Tak et al. 2000b; van Dishoeck & van der Tak 2000). Thus, the fraction of warm over cold gas where H_2O freezes-out is also increased. This suggests that the sources with higher H_2O gas/solid ratios are more evolved than sources with low gas/solid ratios. The sources with the higher gas-phase H_2O abundances and gas/solid ratios also show evidence for thermal processing of the ices (Smith et al. 1989; Boogert et al. 2000; Gerakines et al. 1999). Similarly, other evolutionary tracers, such as gas-phase HCN, C_2H_2, CH_3OH, and CO_2 show their highest abundances and/or gas/solid ratios for the same sources as gas-phase H_2O and the lowest values for those sources where no gas-phase H_2O has been detected (Lahuis & van Dishoeck 2000; van der Tak et al. 2000a; Boonman et al. 2003a). Together, this makes gas-phase H_2O another useful tracer of the evolution of massive protostars.

5.2. Comparison to chemical models

Envelope models by Doty et al. (2002) and hot core models by Charnley (1997) predict enhanced gas-phase H_2O abundances of up to $\sim 10^{-4}$ for $T \gtrsim 230$–300 K in the case of pure gas-phase chemistry. Similar abundances are predicted for $T \gtrsim 100$ K if ice evaporation is included. As noted in Sect. 3, the increasing gas/solid ratios with temperature suggest that ice evaporation is important for our sources. The derived gas-phase H_2O abundances in Table 2 are in agreement with these chemical models.

Shock models by Bergin et al. (1998) and Charnley & Kaufman (2000) show that the H_2O abundance in post-shock gas can also reach values up to $\sim 10^{-4}$. The low spectral resolution of the ISO-SWS data does not allow to derive kinematic information from the observed H_2O lines, making it difficult to distinguish between the envelope/hot core models and shock chemistry. Similarly, a study of sulphur-bearing species, which are thought to be good shock tracers, toward 8 of our sources cannot discriminate between an origin in the shock or warm quiescent gas (Keane et al. 2001a; van der Tak et al. 2003). On the other hand, an analysis of gas-phase CO_2 toward the same sources by Boonman et al. (2003a) suggests that CO_2 was destroyed in $T \sim 100$–300 K gas by the passage of a shock in the past and is either partially destroyed or rapidly reformed through X-ray ionization in $T > 300$ K gas. The results from Sect. 4 do not provide strong evidence for the destruction of H_2O gas after evaporation, but destruction of a small fraction of the gas-phase H_2O in the warm interior cannot be excluded at present. Thus, the inferred results for the ν_2 ro-vibrational band of gas-phase H_2O are not inconsistent with the gas-phase CO_2 results from Boonman et al. (2003a). High spectral-resolution

observations, e.g. with the Heterodyne Instrument for the Far-Infrared (HIFI) on board the Herschel Space Observatory are needed to further investigate the origin of the abundant gas-phase H_2O in massive protostars.

In addition to the high inferred gas-phase H_2O abundances from the infrared absorption bands, SWAS observations of sources in our sample indicate much lower H_2O abundances of $\sim 10^{-9}$ to a few $\times 10^{-8}$ in the outer region (Snell et al. 2000). This suggests that a jump in the H_2O abundance is present for our sources and that the ISO-SWS observations trace primarily the warmer gas in the inner envelope. A similar jump is seen for CH_3OH toward our sources (van der Tak et al. 2000a). In Paper II, the ISO-SWS observations presented here will be combined with the pure rotational H_2O lines observed with ISO-LWS and SWAS in order to find a chemical scenario that can explain all observed H_2O lines between 5 and 540 μm. In Paper II, the three above mentioned processes that can produce high H_2O abundances of 10^{-4}, i.e. high-T gas-phase chemistry, ice evaporation, and shocks, are investigated in more detail.

5.3. Comparison to other sources

ISO-SWS observations of the intermediate-mass protostars AFGL 490 and AFGL 7009S show H_2O abundances of a few $\times 10^{-5}$ (Schreyer et al. 2002; Dartois et al. 1998), while abundances of up to $\sim 10^{-4}$ are found toward Orion-IRc2 (González-Alfonso et al. 1998; Harwit et al. 1998; Wright et al. 2000). These are similar to the abundances inferred for the massive protostars in Sect. 3. Toward the low- to intermediate-mass star-forming regions NGC 1333-IRAS 4 and IRAS 16293-2422 abundances of $(3$–$5) \times 10^{-7}$ for the outer and $(3$–$5) \times 10^{-6}$ for the inner envelope have been derived indicating a jump in the H_2O abundance, similar to what is found for our sources in Sect. 5.2 and Paper II (Maret et al. 2002; Ceccarelli et al. 2000).

6. Conclusions

– The ν_2 ro-vibrational band of gas-phase H_2O has been detected toward 7 of the 12 sources in our sample. Excitation temperatures of $T_{ex} \gtrsim 250$ K are found, indicating an origin in the warm gas.

– Typical gas-phase H_2O abundances of $\sim 5 \times 10^{-6}$–6×10^{-5} are derived from pure absorption models indicating that H_2O is abundant in the warm gas. The abundances increase with the temperature of the warm gas whereas the H_2O ice abundances decrease. However, the gas-phase H_2O abundance in the warmest source is still a factor of ~ 3.5 lower than the ice abundance in the coldest source. Using a more detailed radiative transfer model together with the physical structure of the sources shows that this difference is probably due to emission filling in the absorption lines, which increases the derived gas-phase H_2O abundances by factors of ~ 3–6.

– The inferred gas/solid ratios increase with temperature, suggesting that grain-mantle evaporation is important. The increasing gas/solid ratio correlates with other heating indicators, such as gas-phase HCN, C_2H_2, and CH_3OH.

– Comparison to chemical models shows that envelope models and hot core models can explain the derived gas-phase H$_2$O abundances, but that shock chemistry predicts similar abundances. A more detailed modeling of the gas-phase H$_2$O lines including the physical structure of the objects and different chemical scenarios will be presented in Paper II.

– The derived gas-phase H$_2$O abundances are more than 2 orders of magnitude higher than those derived from SWAS observations toward the same objects, suggesting that a jump in the H$_2$O abundance is present and that the ISO-SWS observations presented here trace primarily the warmer inner envelope.

References

Anthony-Twarog, B. J. 1982, AJ, 87, 1213

Ashby, M. L. N., Bergin, E. A., Plume, R., et al. 2000, ApJ, 539, L119

Azcarate, I. N., Cersosimo, J. C., & Colomb, F. R. 1986, Rev. Mex. Astron. Astrofis., 13, 15

Bergin, E. A., Melnick, G. J., & Neufeld, D. A. 1998, ApJ, 499, 777

Boogert, A. C. A., Ehrenfreund, P., Gerakines, P. A., et al. 2000, A&A, 353, 349

Boonman, A. M. S., van Dishoeck, E. F., Lahuis, F., & Doty, S. D. 2003a, A&A, 399, 1063

Boonman, A. M. S., Doty, S. D., van Dishoeck, E. F., et al. 2003b, A&A, submitted

Ceccarelli, C., Caux, E., Loinard, L., et al. 1999, A&A, 342, L21

Ceccarelli, C., Castets, A., Caux, E., et al. 2000, A&A, 355, 1129

Cernicharo, J., González-Alfonso, E., Alcolea, J., Bachiller, R., & John, D. 1994, ApJ, 432, L59

Charnley, S. B. 1997, ApJ, 481, 396

Charnley, S. B., & Kaufman, M. J. 2000, ApJ, 529, L111

Dartois, E., d'Hendecourt, L., Boulanger, F., et al. 1998, A&A, 331, 651

Doty, S. D., van Dishoeck, E. F., van der Tak, F. F. S., & Boonman, A. M. S. 2002, A&A, 389, 446

Gensheimer, P. D., Mauersberger, R., & Wilson, T. L. 1996, A&A, 314, 281

Gerakines, P. A., Whittet, D. C. B., Ehrenfreund, P., et al. 1999, ApJ, 522, 357

Giannakopoulou, J., Mitchell, G. F., Hasegawa, T. I., Matthews, H. E., & Maillard, J.-P. 1997, ApJ, 487, 346

Gibb, E. L., & Whittet, D. C. B. 2002, ApJ, 566, L113

González-Alfonso, E., Cernicharo, J., van Dishoeck, E. F., Wright, C. M., & Heras, A. 1998, ApJ, 502, L169

Harwit, M., Neufeld, D. A., Melnick, G. J., & Kaufman, M. J. 1998, ApJ, 497, L105

Helmich, F. P., van Dishoeck, E. F., Black, J. H., et al. 1996, A&A, 315, L173

Henning, Th., Pfau, W., & Altenhoff, W. J. 1990, A&A, 227, 542

Henning, T., Chini, R., & Pfau, W. 1992, A&A, 263, 285

Keane, J. V., Boonman, A. M. S., Tielens, A. G. G. M., & van Dishoeck, E. F. 2001a, A&A, 376, L5

Keane, J. V., Tielens, A. G. G. M., Boogert, A. C. A., Schutte, W. A., & Whittet, D. C. B. 2001b, A&A, 376, 254

Lacy, J. H., Knacke, R., Geballe, T. R., & Tokunaga, A. T. 1994, ApJ, 428, L69

Lahuis, F., & van Dishoeck, E. F. 2000, A&A, 355, 699

Maret, S., Ceccarelli, C., Caux, E., Tielens, A. G. G. M., & Castets, A. 2002, A&A, 395, 573

Mitchell, G. F., Maillard, J.-P., Allen, M., Beer, R., & Belcourt, K. 1990, ApJ, 363, 554

Mueller, K. E., Shirley, Y. L., Evans, N. J. II, & Jacobson, H. R. 2002, ApJS, 143, 469

Nisini, B., Benedettini, M., Giannini, T., et al. 1999, A&A, 350, 529

Persi, P., Ferrari-Toniolo, M., & Spinoglio, L. 1987, in Circumstellar matter, ed. I. Appenzeller, & C. Jordan (Dordrecht: Reidel), IAU Symp., 122, 93

Phillips, T. G., Kwan, J., & Huggins, P. J. 1980, in Interstellar Molecules, ed. B. H. Andrew (Dordrecht: Reidel), IAU Symp., 87, 21

Schreyer, K., Henning, Th., van der Tak, F. F. S., Boonman, A. M. S., & van Dishoeck, E. F. 2002, A&A, 394, 561

Smith, R. G., Sellgren, K., & Tokunaga, A. T. 1989, ApJ, 344, 413

Snell, R. L., Howe, J. E., Ashby, M. L. N., et al. 2000, ApJ, 539, L101

Tauber, J., Olofsson, G., Pilbratt, G., Nordh, L., & Frisk, U. 1996, A&A, 308, 913

Thompson, R. I., Thronson, H. A., Jr., & Campbell, B. G. 1981, ApJ, 249, 622

van der Tak, F. F. S., 2000, Ph.D. Thesis, Leiden University

van der Tak, F. F. S., van Dishoeck, E. F., & Caselli, P. 2000a, A&A, 361, 327

van der Tak, F. F. S., van Dishoeck, E. F., Evans, N. J., II, & Blake, G. A. 2000b, ApJ, 537, 283

van der Tak, F. F. S., Boonman, A. M. S., Braakman, R., & van Dishoeck, E. F. 2003, A&A, submitted

van Dishoeck, E. F., & Helmich, F. P. 1996, A&A, 315, L177

van Dishoeck, E. F. 1998, in Chemistry and Physics of Molecules and Grains in Space, Faraday Discussions, 109, 31

van Dishoeck, E. F., & van der Tak, F. F. S. 2000, in Astrochemistry: From Molecular Clouds to Planetary Systems, ed. Y. C. Minh, & E. F. van Dishoeck (San Francisco: Astron. Soc. Pac.), IAU Symp. 197, 97

Wright, C. M., van Dishoeck, E. F., Black, J. H., et al. 2000, A&A, 358, 689

Zmuidzinas, J., Blake, G. A., Carlstrom, J., et al. 1995, in Airborne Astronomy Symposium on the Galactic Ecosystem: From Gas to Stars to Dust, ed. M. R. Haas, J. A. Davidson, & E. F. Erickson (San Francisco: Astron. Soc. Pac.), ASP Conf. Ser., 73, 33